VOL. 11, NO. 12, JUNE 2016 ISSN 1819-6608
ARPN Journal of Engineering and Applied Sciences


www.arpnjournals.com

# AN INVESTIGATION IN RADIAL GAP AIR-RIDING SEALS FOR AERO-ENGINES

Shubham Kumar, Seamus Garvey and Hervé Morvan
The University of Nottingham, Nottingham, United Kingdom
E-Mail: Shubham.Kumar@nottingham.ac.uk

**ABSTRACT**

With the aero-engine manufacturers aiming for Operating Power Ratios (OPRs) higher than 50:1 and improved engine efficiency, the capabilities of the present sealing systems are bound to be severely tested. Air riding seals have emerged as potential candidates to deal effectively with the high pressure discharge air from the compressor. The simplest types of air-riding seals are those with an axial gap. Radial gap seals can provide another level of advantage in terms of their applicability and the total axial travel that needs to be accommodated. This paper provides an overview on a preliminary design effort in modelling and designing a radial gap air riding seal having a continuous ring structure. It investigates a key issue regarding these seals: developing a positive radial stiffness in the air-film to drive the sealing ring to accommodate for any radial shaft movement while maintaining a minimum clearance from the shaft to avoid any contact (in effect, having sort of a bearing-like action). The paper discusses the results from 1D and 2D analyses of the flow through a small sector of the seal, and demonstrates a methodology to calculate the stiffness and damping coefficients of the fluid-film. This is followed by steady state and transient CFD simulations to further analyse the characteristics of this fluid film and understand the time-constants associated with perturbations of the film.

**Keywords:** aero-engines, air riding seals, stiffness, fluid dynamics, leakage, stability, rotordynamics.

## INTRODUCTION

The aviation industry has been one of the most prolific sectors of development over the last 10-15 years. Passenger traffic as measured by revenue passenger kilometers (RPK) is expected to rise by 4.9% each year for the next two decades, thus leading to a need of around 38,050 aircrafts [1]. The rise in aircraft demand would also imply a significant rise in aero-engine demand to power these aircrafts. The Rolls-Royce Market Outlook [2] predicts a requirement of 55,000 engines over the next decade, generating around 1,600 million pounds of installed thrust.

Most of the aero-engine manufacturers are in pursuit of technologies that show promise of high performance to cost benefit ratios. To obtain the low Specific Fuel Consumption (SFC) desired for the next-gen engines, more progress must be made in increasing core efficiencies. Advanced engine seals show promise of reducing engine losses and maintaining these performance benefits over the service interval of the engine. Studies performed by [3], and supported by [4], estimated that making the same performance improvements by improving seal technology would cost 4 to 5 times less than that brought about by improving the present compressors or turbines by other means.

Air riding seals rely on a thin film of air to separate the seal faces and they show promise of reducing wear and leakage to its practical limit. These seals can be designed to operate at the high pressures and temperatures anticipated for next-generation gas turbine engines. There are two classes of film riding seals being developed for gas turbines: hydrostatic and hydrodynamic seals. Hydrostatic face seals port high pressure fluid to the sealing face to induce opening force and to maintain controlled face separation. Hydrodynamic or self-acting face seals incorporate lift pockets to generate a hydrodynamic film between the two faces to prevent seal contact. Hydrodynamic seals operate on extremely small clearances, resulting in very low leakage compared to labyrinth or brush seals [5].

The prior art in the field of radial gap seals (or circumferential seals, as they are sometimes referred to) comprises of segmented seals, such as Stein seals [6], where the seal ring is formed by a plurality of circumferential segments placed end to end and held together by means of a garter spring. Each segment in the inner circumferential face includes at least one pumping groove which provides a negative hydrodynamic lift force which tends to move the seal ring segments toward the shaft to reduce leakage. As these seals are contact-type seals, where the air pressure unloads the contact between the seal and the shaft, they cannot be called as air-riding seals.

This paper provides an overview on a preliminary design effort in modelling a new category of seals – a continuous ring-type radial gap air-riding seal. A ring like structure acts as the primary seal, through the formation of an extremely thin film of air between the stator (seal ring) and the rotor (shaft). The seal benefits from both hydrostatic and hydrodynamic film generation features due to the rotation of the shaft and high differential pressure across the axial ends of the seal. One of the challenges concerning this type of seal would be to maintain a positive clearance from the shaft when there is a differential growth of the seal ring and the shaft (due to heat or high shaft rotation speed). This paper presents the observation and results from an initial investigation of the fluid film formed between the stator and rotor. 1D and 2D finite difference analyses are carried out on a small sector (1 degree) of the seal to analyse the various flow

characteristics. This is followed by steady state and transient CFD simulations on the fluid film to get a more detailed analysis of the flow parameters.

## SEAL ASSEMBLY

Figure-1 shows an envisaged set-up of a test-rig of the seal assembly. The seal assembly includes a housing 8, which comprises of an inlet chamber 8a and an outlet chamber 8b. One end of the shaft (rotor) 3 and the radial gap air-riding seal (primary seal) 7, are mounted in housing. The primary seal is secured to the housing 8 by a holding assembly 6, which also acts as a secondary seal. The shaft is supported by ball bearings 5 at each end of the housing, and the inlet chamber of the housing is sealed by a contact-type seal 4. The other end of the shaft is connected to a motor 1 through a coupling 2. It should be understood that all the elements of the assembly listed above are annular and dimensionally exaggerated for ease of understanding, and Figure-1 just shows the front-view of the assembly.

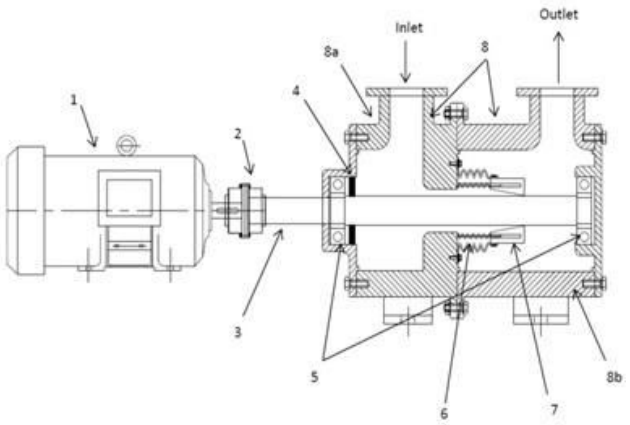


**Figure-1.** Seal assembly.

High pressure air from a compressor is fed into the inlet chamber through the inlet port. The pressurized air then passes through the primary & secondary seal arrangement to the outlet chamber, and finally exits through the low pressure outlet port. The mean seal gap between the seal ring and the shaft is ~32 µm, which ensures a very small leakage rate through the seal. Due to the hydrostatic and hydrodynamic lift generation brought about by the differential pressure across the seal and the shaft rotation, an extremely thin fluid film is developed in the seal gap. It is absolutely essential to ensure that the seal ring is able to follow the rotor in its radial movement, which would require the fluid film to be stiff enough to move the seal ring with itself. The secondary seal arrangement supports and guides the primary seal ring along its axial and radial movements.

## SEAL GEOMETRY AND 1D ANALYIS

Figure-2 shows the axial seal gap geometry of the seal. A converging-gap geometry was selected in order to ensure positive lift generation through hydrostatic means. For the convenience of analysis, the axial seal gap is divided into 10 sub-lengths, and the inlet and outlet end of each of these sub-lengths are termed as nodes. As difference in seal gap height for two consecutive sub-lengths is just 4µm, it is assumed that there is no significant pressure loss between the outlet of a sub-length and the inlet of the subsequent sub-length. So the outlet of a sub-length and the inlet of the subsequent sub-length are considered to be one node. This implies that there are 11 seal nodes, if the axial seal gap is divided into 10 sub-lengths.

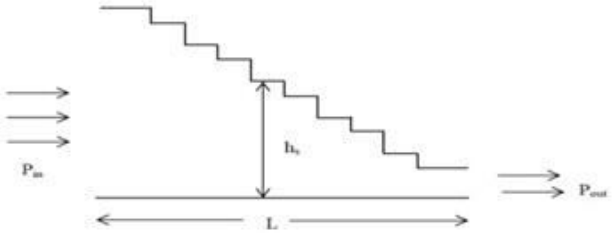


**Figure-2.** Seal gap geometry.

In Figure-2, $L$ denotes the total length of the seal in the axial direction, $h_n$ represents the height of the $n^{th}$ sub-length, and $P_{in}$ & $P_{out}$ denote the inlet and outlet pressure respectively. All the analyses reported in this paper have been performed with a $P_{in}$ of 10 bar and a $P_{out}$ of 1 bar. The maximum seal height $h_1$ (at seal inlet) is 50µm and the minimum seal height $h_{10}$ (at seal outlet) is 14µm.

It is considered that the shaft is perfectly centred, so there is no circumferential variation of seal height. Hence, the flow is purely axial in this case. The flow rate through each seal sub-length can then be calculated by using Poiseuille's flow equation [7]. The pressure at each node of the axial seal length can then be computed as:

$$P_{i+1} = P_i - \frac{12\mu L\dot{m}}{\rho_i w h_i^3} \qquad \{i \in \mathbb{Z} \mid 1 \leq i \leq 10\} \tag{1}$$

where, $\dot{m}$ is the mass flow rate, $h_i$ and $\rho_i$ are respectively the seal gap height and density of air in the $i^{th}$ sub-length, $P_i$ and $P_{i+1}$ are the pressures at the $i^{th}$ and $(i+1)^{th}$ node respectively, $w$ is circumferential length of the seal sector, $L$ is the axial seal length, and $\mu$ is the coefficient of viscosity of air. The density of air is corrected for each sub-length by considering air as an ideal gas.

To ensure that there is positive hydrostatic lift generation, the shaft is considered to be shifted upwards by a small amount $\Delta h$ (1 micron) and subsequent changes in pressure in each sub-length are then computed for a small sector of the seal (1° sector).

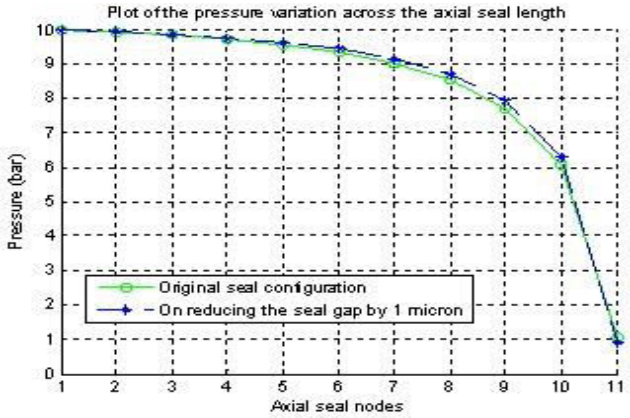


**Figure-3.** Plot of the pressure variation across the seal length.

It may be observed from Figure-3 that there is an increase in pressure in each seal sub-length on decreasing the seal gap by 1 micron. This confirms that the fluid film exhibits positive lift generation.

## 2D ANALYSIS

As the geometry and working principle of the radial-gap seal is very similar to a gas bearing, Reynold's equation for flow in gas bearings is used as the governing equation to characterise the fluid flow in the seal. Similar to the case of 1D analysis, a 1° sector of the full seal is analysed and it is assumed that the shaft is centred. For a steady-state condition, the non-dimensional form of the Reynold's equation for lubrication can be expressed as [8]:

$$\frac{\partial}{\partial X}\left(H^3 P \frac{\partial P}{\partial X}\right) + \frac{\partial}{\partial Z}\left(H^3 P \frac{\partial P}{\partial Z}\right) = \Lambda \frac{\partial (PH)}{\partial X} \quad (2)$$

where, $X = \frac{x}{a}$, $Z = \frac{z}{a}$, $P = \frac{p}{p_a}$, $H = \frac{h}{\Delta}$, $\Lambda = \frac{6\mu a U_0}{p_a \Delta^2}$

A central finite difference scheme with a uniform grid was used to solve this non-dimensional equation, with the relevant boundary conditions.

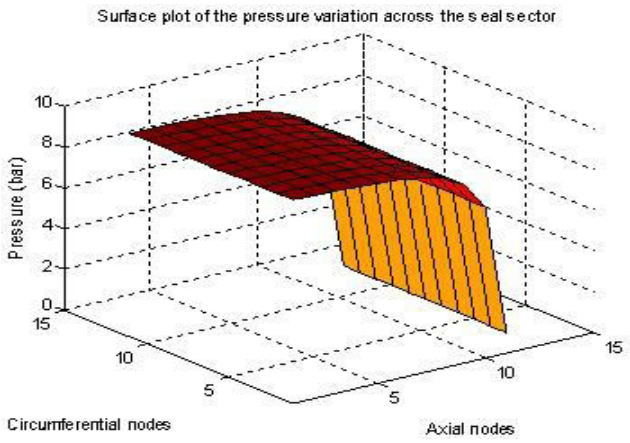


**Figure-4.** Surface plot of the pressure variation across the seal for a static shaft (Hydrostatic).

Figure-4 shows the surface plot for the pressure variation obtained through the 2D finite difference model developed for the non-dimensional Reynold's equation. It should be noted that the above result is obtained for a hydrostatic case as the shaft is kept static here.

The shaft is then given a rotational speed of 10,000rpm. Although the pressure plots, in the case of a static and a moving shaft, look quite similar, it is observed that there is a very slight increase in pressure variation across the seal when the shaft is rotated about its axis at 10,000rpm, which can be attributed to the hydrodynamic lift generation in the fluid film. Since the mean seal height is so small (~32µm) and the analysis has been performed for just a small sector of the whole seal ring, the contribution of hydrodynamic lift to the overall lift force is not very significant, as it may be observed from Figure-5.

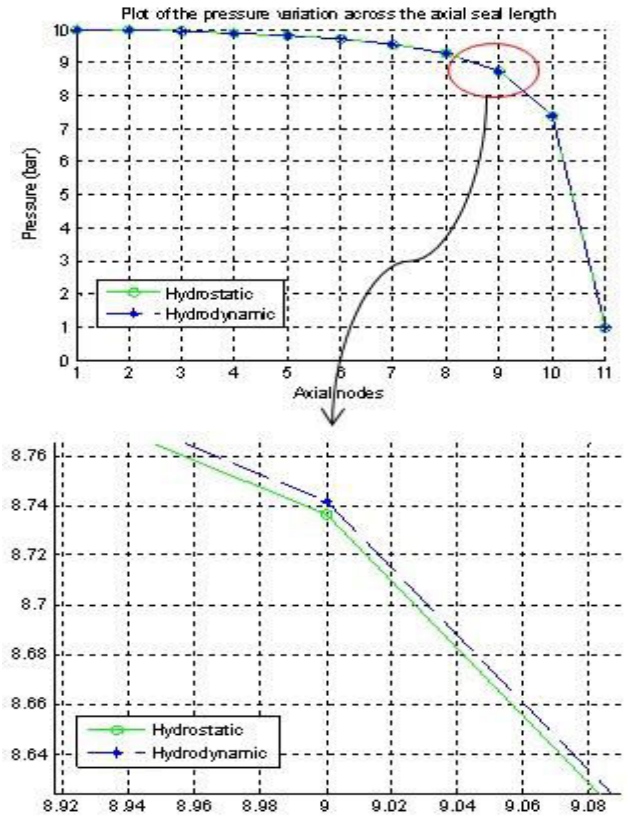


**Figure-5.** Plot of Pressure variation across the seal length in hydrostatic and hydrodynamic case.

## CFD ANALYSIS

Following the analysis on Reynold's equation, CFD simulations of the fluid film are carried out. Initially, steady state simulations are carried out to compare the results with 2D simulations. The CFD simulations are performed on ANSYS-CFX. The Shear Stress Transport (SST) model is used for modelling the turbulence, and high speed numeric option is enabled. The shaft is treated as a rotating wall and rotational periodicity is implemented on the side walls of the fluid film. Figure-6 shows a plot to

compare the pressure variations computed from the 2D and CFD analysis.

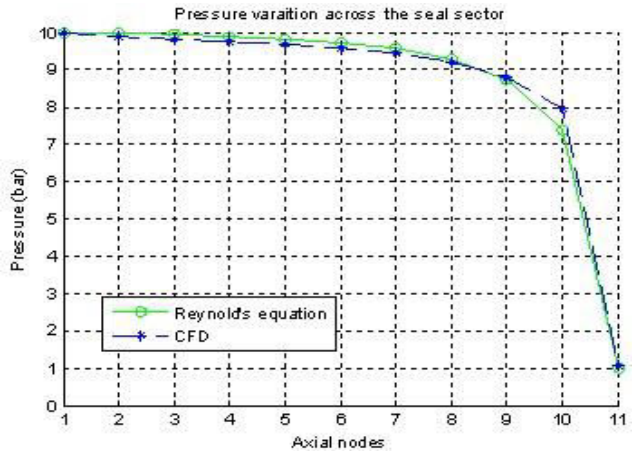


**Figure-6.** Comparison between the results from 2D and CFD analyses

## ROTORDYNAMIC ANALYSIS OF THE FLUID FILM

To understand the seal dynamics it is essential to understand the stiffness and the damping characteristics of the fluid film. The equation of motion for a mass-spring-damper model can be written as:

$$[M]\{\ddot{x}\} + [C]\{\dot{x}\} + [K]\{x\} = \{f\} \quad (3)$$

where, $[M]$, $[C]$ and $[K]$ are mass, damping and stiffness matrices respectively, and $\{f\}$ is the external force applied.

As shown in Figure-1, the axial movement of the seal is constrained by the secondary seal arrangement. Hence, it will have two degrees of freedom in the radial plane. As the studies in this paper are based on a small sector of the full seal geometry, the discussion on rotordynamics of the full seal will be considered to be outside the scope of this paper.

For a 2D analysis on a sector of the seal, there is just one realistic degree of freedom, i.e. the movement along a direction normal to the axial surface. In this paper, just for the sake of discussion, it will be considered that the seal ring is free to rotate about the low pressure end. This would imply that there will be another degree of freedom in terms of an angular movement of the seal.

In order to compute the stiffness coefficients, the shaft is moved up radially by 1 micron and the resulting rise in lift force, and the moment about the low pressure end, is evaluated for each axial sub-length of the seal. Similarly, the low pressure end of the seal is then rotated by 1° and the subsequent changes in moments and lift force are computed for each seal sub-length. The stiffness matrix is thus evaluated as:

$$K = 1 \times 10^5 \begin{bmatrix} 1.21233 & -0.00321 \\ 0.00405 & -0.00001 \end{bmatrix} \quad (4)$$

The damping matrix is calculated in a similar manner. The shaft is perturbed radially by 1m/s and it is rotated about the low pressure end by 1rad/s, and the resulting change in downstream and upstream flow is calculated by considering the dissipation in each case. Hence a flow regime for minimum dissipation is evaluated. Accordingly, the mass flow rate in both directions is estimated and the subsequent change in force and momentum for each seal sub-length is calculated to formulate the damping matrix. The damping matrix is thus computed as:

$$C = 1 \times 10^4 \begin{bmatrix} 5.20244 & -0.01722 \\ 0.01758 & -0.00006 \end{bmatrix} \quad (5)$$

## TRANSIENT CFD ANLYSIS FOR TIME-CONSTANT STUDY

To study the time-constants associated with the fluid film, the film is given a small perturbation in the radial direction by giving an initial velocity of 0.05 m/s to the shaft in the radial direction. This is simulated as a transient analysis on CFX by treating the shaft surface as a 'rigid body' and the mesh deformation conditions for the various boundaries are set in such a way so that they are coherent with the solution of the rigid body movement. The lift force acting on the fluid film is then plotted against time. The initial "noise" from the transients is filtered out (truncated) and the force values are fitted to a curve as per a modified decay equation Eqn.(6) using Levenberg-Marquardt algorithm. A cosine and sine decay function is introduced as it is observed from the force values that there is a small oscillation in its decay behavior.

$$f(t) = a + b\left(e^{-t/\tau_b}\right) + e^{-t/\tau_c}(c\cos\omega t + d\sin\omega t) \quad (6)$$

where, $\tau_b$ and $\tau_c$ are the time constants associated with the function *f(t)*.

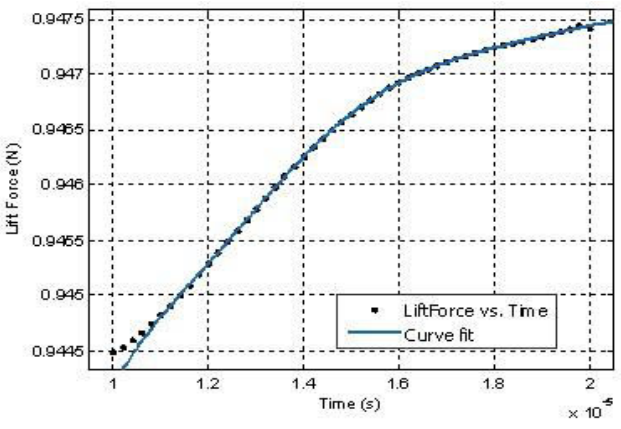


**Figure-7.** Curve fitting the decay function for lift force.

Table-1 shows the results from curve fitting the decay equation to the force transients on perturbing the shaft.

**Table-1.** Results from curve fitting.

| Variable | Value |
|---|---|
| $\tau_b$ | 3.984 x$10^{-6}$ s |
| $\tau_c$ | 2.617 x$10^{-6}$ s |
| $a$ | 0.9478 N |
| $b$ | -0.0489 N |
| $c$ | -0.0171 N |
| $d$ | 0.0004029 N |
| $\omega$ | 9.362 x $10^5$ rad/s |

## CONCLUSIONS

A suitable layout of the seal assembly was designed and a small sector of the fluid film, formed in the axially converging seal gap, was analysed to calculate the flow parameters through the sector.

- Positive lift generation of the fluid film through hydrostatic and hydrodynamic means was confirmed through 1D and 2D analyses.
- There was a good correlation between the results from 2D finite difference analysis model and the CFD simulation.
- The full seal geometry needs to be analysed through CFD simulations to capture both the realistic degrees of freedom in order to formulate the stiffness and damping matrices.
- As it can be observed from Table-1, the time-constants associated with the perturbations of fluid film are of the order of $10^{-6}$ seconds. Since structural vibrations and instabilities rarely, if ever, reach such high frequencies, the fluid film should be able to maintain a minimum clearance from the shaft for any realistic perturbations.

## ACKNOWLEDGEMENTS

The research leading to these results has received funding from the People Programme (Marie Curie Actions) of the European Union's Seventh Framework Programme (FP7/2007-2013) under REA grant agreement no 608322. The authors would also like to thank Corac Energy Technologies Limited for their guidance and inputs during this research.

## REFERENCES

[1] http://www.boeing.com/resources/boeingdotcom/commercial/about-our-market/assets/downloads/Boeing_Current_Market_Outlook_2015.pdf. (2015, February 14). Boeing - Current Market Outlook 2015.

[2] http://www.rolls-royce.com/products-and-services/civil-aerospace/customer-focus/market-outlook.aspx. (2014, February 12). Civil Aerospace-Market Outlook.

[3] H. Stocker, D. Cox, and G. Holle, "Aerodynamic performance of conventional and advanced design labyrinth seals with solid-smooth abradable, and honeycomb lands. [gas turbine engines]," 1977.

[4] C. J. Smith, "Unique Propulsion Systems Advanced Subsonic Technologies Evaluation and Analysis,"" 1994.

[5] J. H. Munson, "Testing of a high performance compressor discharge seal," in Joint Propulsion Conference and Exhibit, 1993.

[6] M. R. Borkiewicz, "Segmented hydrodynamic seals for sealing a rotatable shaft," US5509664 A, 1996.

[7] A. T. M. Robert W. Fox, Philip J. Pritchard, " Introduction to Fluid Mechanics ", 6th ed: John Wiley & Sons, Inc., 2004, pp. 310 - 315.

[8] Z. Szeri, "Fluid film lubrication," vol. 1, ed: Cambridge University Press, 2011, pp. 451 - 456.